



# The Origin of High Activity of Amorphous MoS<sub>2</sub> in the Hydrogen Evolution Reaction

Longfei Wu,<sup>[a]</sup> Alessandro Longo,<sup>[b]</sup> Nelson Y. Dzade,<sup>[c, d]</sup> Akhil Sharma,<sup>[e]</sup> Marco M. R. M. Hendrix,<sup>[f]</sup> Ageeth A. Bol,<sup>[e]</sup> Nora H. de Leeuw,<sup>[c, d]</sup> Emiel J. M. Hensen,<sup>\*,[a]</sup> and Jan P. Hofmann<sup>\*,[a]</sup>

Molybdenum disulfide (MoS<sub>2</sub>) and related transition metal chalcogenides can replace expensive precious metal catalysts such as Pt for the hydrogen evolution reaction (HER). The relations between the nanoscale properties and HER activity of well-controlled 2H and Li-promoted 1T phases of MoS<sub>2</sub>, as well as an amorphous MoS<sub>2</sub> phase, have been investigated and a detailed comparison is made on Mo–S and Mo–Mo bond analysis under operando HER conditions, which reveals a similar bond structure in 1T and amorphous MoS<sub>2</sub> phases as a key feature in explaining their increased HER activity. Whereas the distinct bond structure in 1T phase MoS<sub>2</sub> is caused by Li<sup>+</sup> intercalation and disappears under harsh HER conditions, amorphous MoS<sub>2</sub> maintains its intrinsic short Mo–Mo bond feature and, with that, its high HER activity. Quantum-chemical calculations indicate similar electronic structures of small MoS<sub>2</sub> clusters serving as models for amorphous MoS<sub>2</sub> and the 1T phase MoS<sub>2</sub>, showing similar Gibbs free energies for hydrogen adsorption ( $\Delta G_{H^+}$ ) and metallic character.

Scalable electrochemical proton reduction (hydrogen evolution reaction, HER) is crucial for realizing large-scale storage of renewable energy. Water splitting requires efficient and robust catalysts, which are composed of earth-abundant elements. The most active metal catalyst for HER is Pt, which is scarce and thus makes scale-up of water electrolysis to terawatt (TW) scale too costly.<sup>[1]</sup> Molybdenum disulfide (MoS<sub>2</sub>), one of the most studied transition metal chalcogenides (TMCs), has received substantial attention because of its unique physiochemical properties, such as a tunable band gap,<sup>[2]</sup> high catalytic ac-

tivity,<sup>[3]</sup> and high electron mobility.<sup>[4]</sup> These properties allow it to be exploited in transistors,<sup>[5]</sup> metalloenzymes,<sup>[6]</sup> and, at a practical scale, as the active phase in industrial catalysts for hydrotreatment of oil fractions.<sup>[7]</sup> The ability to activate hydrogen reversibly also explains its promise for catalyzing hydrogen evolution in the context of electrochemical water splitting.<sup>[8]</sup> Not surprisingly, the edge sites of MoS<sub>2</sub> nanocatalysts have been identified as active HER sites by Jaramillo and co-workers.<sup>[9]</sup> Since then, tremendous efforts have been devoted to engineering the surface structure of MoS<sub>2</sub> to preferentially expose these edge sites to improve HER performance.<sup>[10]</sup>

Different polymorphs of MoS<sub>2</sub> exist in the form of 2H (trigonally coordinated), 1T (octahedrally coordinated), and 3R phases (rhombohedral).<sup>[3,11]</sup> 2H-MoS<sub>2</sub> is the thermodynamically stable two-dimensional (2D) phase with semiconductor properties (band gap  $\approx$  1.9 eV for monolayer, 1.2 eV for bulk),<sup>[12]</sup> a low electron mobility, and a limited number of HER-active (edge) sites. These properties render this phase less attractive for electrocatalytic applications<sup>[2,13]</sup> than the octahedral 1T phase, which is metallic and six orders of magnitude more conductive.<sup>[13a]</sup> The improved charge transfer kinetics and the affinity for binding H atoms on 1T-MoS<sub>2</sub> are reported to be responsible for the substantially enhanced HER activity compared to the 2H phase. However, the underlying mechanism of the high HER activity of the 1T phase has yet to be elucidated.<sup>[14]</sup> As the 1T phase can be formed from 2H-MoS<sub>2</sub> by intercalation of cations (e.g., Li<sup>+</sup>, Na<sup>+</sup>),<sup>[15]</sup> it is usually characterized by distorted structural domains.<sup>[16]</sup> Aside from 2H and 1T phases, amorphous MoS<sub>x</sub> ( $x=2-3$ ) has also been extensively investigated in the past as a hydrotreatment catalyst and as a cathode materi-

[a] Dr. L. Wu, Prof. Dr. E. J. M. Hensen, Dr. J. P. Hofmann  
Laboratory for Inorganic Materials and Catalysis  
Department of Chemical Engineering and Chemistry  
Eindhoven University of Technology  
P.O. Box 513, 5600 MB Eindhoven (The Netherlands)  
E-mail: E.J.M.Hensen@tue.nl  
J.P.Hofmann@tue.nl


[b] Dr. A. Longo  
Netherlands Organization for Scientific Research (NWO)  
The European Synchrotron Radiation Facility (ESRF)  
CS40220, 38043 Grenoble Cedex 9 (France)


[c] Dr. N. Y. Dzade, Prof. Dr. N. H. de Leeuw  
Faculty of Geosciences, Utrecht University  
Princetonplein 9, 3584 CC Utrecht (The Netherlands)

[d] Dr. N. Y. Dzade, Prof. Dr. N. H. de Leeuw  
School of Chemistry, Cardiff University  
Main Building, Park Place, CF10 3AT, Cardiff (UK)

[e] Dr. A. Sharma, Prof. Dr. A. A. Bol  
Department of Applied Physics, Eindhoven University of Technology  
P.O. Box 513, 5600 MB Eindhoven (The Netherlands)

[f] M. M. R. M. Hendrix  
Laboratory of Physical Chemistry  
Department of Chemical Engineering and Chemistry  
Eindhoven University of Technology  
P.O. Box 513, 5600 MB Eindhoven (The Netherlands)

 Supporting Information (including experimental details) and the ORCID identification number(s) for the author(s) of this article can be found under:  
<https://doi.org/10.1002/cssc.201901811>.

 © 2019 The Authors. Published by Wiley-VCH Verlag GmbH & Co. KGaA. This is an open access article under the terms of the Creative Commons Attribution License, which permits use, distribution and reproduction in any medium, provided the original work is properly cited.

al in lithium-ion batteries.<sup>[17]</sup> Furthermore, it was recently reported by Hu and other groups that this form of MoS<sub>2</sub> is a highly active electrocatalyst for HER.<sup>[8b,18]</sup> Although Mo edge sites of 2H-MoS<sub>2</sub> have been experimentally identified as the active HER sites, the question of what causes the superior catalytic performances of 1T and amorphous phase MoS<sub>2</sub> remains unclear, which adds to the challenge of unraveling the HER mechanism in amorphous MoS<sub>2</sub>.<sup>[11,17b,c,19]</sup>

Here, we show how the structure and surface properties of 2H, 1T, and amorphous MoS<sub>2</sub> influence the HER activity and stability by a combined theory as well as ex situ and operando X-ray spectroscopy approach. In comparison to 2H-MoS<sub>2</sub>, shorter Mo–S and Mo–Mo bonds were observed in both 1T and amorphous MoS<sub>2</sub> thin film electrodes. Besides, both core level Mo 3d and valence band photoemission spectra indicate that 1T and amorphous phase MoS<sub>2</sub> exhibit a similar electronic structure. The short Mo–Mo bond in 1T phase MoS<sub>2</sub> is caused by lithium intercalation and gradually changes back to the 2H phase accompanied by a decrease in HER activity at high overpotentials. By contrast, amorphous MoS<sub>2</sub> (Am-MoS<sub>2</sub>) retains its intrinsic (short) Mo–S and Mo–Mo bond structure as well as high HER activity after 24 h electrochemical testing under the same conditions. Electrochemical operando X-ray absorption spectroscopy was performed to probe the local bond and electronic structure of MoS<sub>2</sub> under HER conditions. The results show that the observed short Mo–Mo bonds play a key role in determining the activity of both 1T and amorphous phase MoS<sub>2</sub> electrocatalysts for HER.

2H and amorphous MoS<sub>2</sub> films were prepared by plasma-enhanced atomic layer deposition (PEALD) on glassy carbon plates at 450 and 250 °C, respectively, whereas the 1T phase was synthesized by lithium intercalation of the as-deposited 2H-MoS<sub>2</sub> (see the Supporting Information for details). The HER electrocatalytic activity of as-prepared MoS<sub>2</sub> films was assessed in 0.1 M H<sub>2</sub>SO<sub>4</sub> in a typical three-electrode electrochemical cell. As shown in Figure 1, both cyclic voltammetry (CV) and linear sweep voltammetry (LSV) curves present higher current densities for 1T and amorphous MoS<sub>2</sub>, as compared to the 2H phase. However, even though 1T and amorphous MoS<sub>2</sub> have comparable current densities initially, the catalytic activity of the 1T phase gradually decreases during the stability test, whereas Am-MoS<sub>2</sub> maintained its higher initial activity (Figure 1d). This particular behavior led us to investigate further the electronic and structural properties of the materials.

We used X-ray absorption spectroscopy at the Mo K-edge to probe the electronic as well as local geometric structure of these films. Ex situ X-ray absorption near-edge spectra (XANES) of MoS<sub>2</sub> films before and after HER stability tests recorded under a grazing incidence angle of 0.3° (grazing incidence X-ray absorption spectroscopy)<sup>[23]</sup> are shown in Figure 2. The suppression of features A and D in 1T (Figure 2d) compared to 2H-MoS<sub>2</sub> emphasizes its distinct bond structure. Importantly,

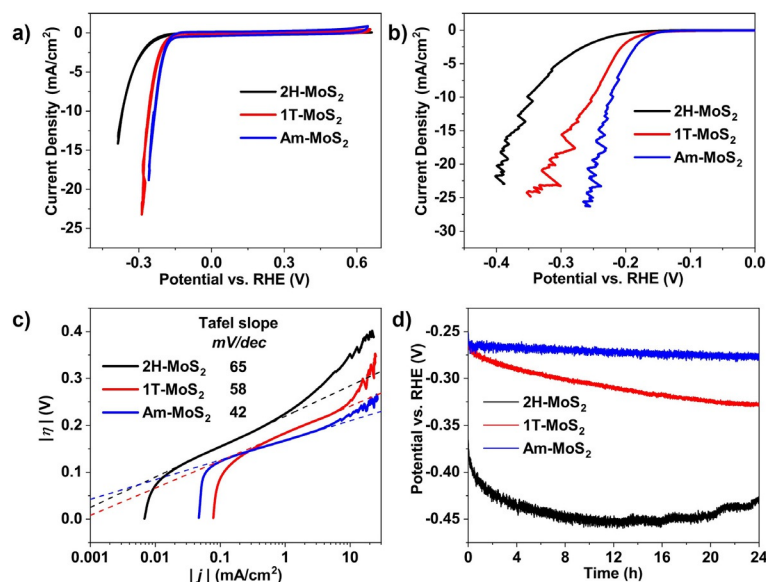


**Figure 1.** a, b) Cyclic voltammetry (CV; a) and linear sweep voltammetry (LSV; b) curves of 2H-, 1T-, and Am-MoS<sub>2</sub> films corrected by uncompensated resistance with scan rates of 50 mV s<sup>-1</sup> for CV and 5 mV s<sup>-1</sup> for LSV. c) Tafel slopes obtained from LSV curves in (b). d) Chronopotentiometric responses (V–t) recorded at a constant current density of 3 mA cm<sup>-2</sup>. Electrolyte: 0.1 M H<sub>2</sub>SO<sub>4</sub>.

features A and D reappear for 1T-MoS<sub>2</sub> after 24 h HER stability testing, which implies that the 1T phase is not stable under the HER conditions and gradually changes back to 2H-MoS<sub>2</sub>. Feature D is absent for the amorphous phase MoS<sub>2</sub> both before and after the HER, indicating its stable bond structure (Figure 2g), which is in contrast to 2H-MoS<sub>2</sub>. Absorption edge features in the XANES spectra are very sensitive to the electronic properties of the atoms being probed:<sup>[20]</sup> the less expressed shoulder at the edge and the shift of the white line for 1T-MoS<sub>2</sub> compared to 2H-MoS<sub>2</sub> are indicative of the structural differences. Simulations of the Mo-K edge XANES spectra of MoS<sub>2</sub> with hexagonal (2H phase) and monoclinic (1T phase with Li intercalation) symmetry were performed to understand these differences. The red curves (Figure 2j, k) represent calculated spectra based on the model structure and the blue curves are calculated taking into account broadening by core-hole lifetime effects.<sup>[21]</sup> The fitted XANES spectra in both cases reproduce the experimental features of 2H- and 1T-MoS<sub>2</sub> well, which confirms their assignment. As monoclinic MoS<sub>2</sub> shows octahedral Mo coordination with a shorter bond distance than 2H-MoS<sub>2</sub> upon Li intercalation, we may conclude that the as-prepared 1T-MoS<sub>2</sub> in this study has a distorted bond structure. For further comparison, ex situ grazing incidence extended X-ray fine structure (GI-EXAFS) data of MoS<sub>2</sub> films were recorded before and after stability measurements. The Fourier transform (FT) profiles in R-space (Figure 2b, c) present two main peaks at 2.40 Å and 3.16 Å (Table 1) corresponding to the nearest Mo–S and Mo–Mo bonds, respectively. The coordination number (CN) values shown in Table 1 suggest that there is no complete shell of S atoms around the central Mo at the surface of the MoS<sub>2</sub> films, which can be due to termination by Mo edges or oxidation by emersion from the electrolyte and air ex-

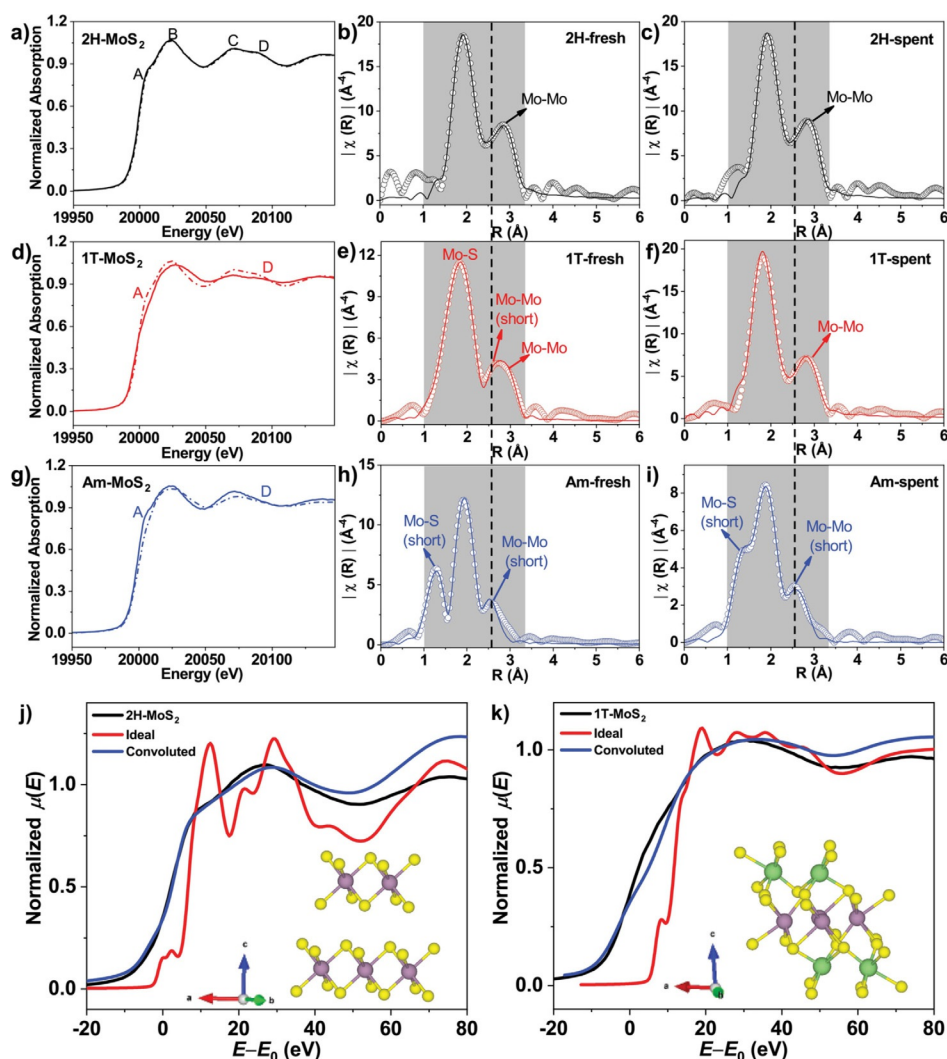


**Figure 2.** a, d, g) Mo K-edge XANES spectra of 2H-MoS<sub>2</sub> (a), 1T-MoS<sub>2</sub> (d), and Am-MoS<sub>2</sub> (g) before (solid line) and after (dash line) stability test. b, e, h) Mo K-edge Fourier transform EXAFS ( $k^3$ -weighted) of 2H-MoS<sub>2</sub> (b), 1T-MoS<sub>2</sub> (e), and Am-MoS<sub>2</sub> (h) before stability test. c, f, i) Mo K-edge Fourier transform EXAFS ( $k^3$ -weighted) of 2H-MoS<sub>2</sub> (c), 1T-MoS<sub>2</sub> (f), and Am-MoS<sub>2</sub> (i) after stability test. j, k) Mo K-edge XANES spectra of experimental data (black curve) and calculated simulation based on hexagonal (j, inset) and monoclinic (k, inset) structure model (purple, yellow, and green balls corresponds to Mo, S, and Li atoms, respectively); red curves represent simulated spectra whereas blue curves represent simulated spectra convoluted with the Mo 1s core-hole lifetime.

posure.<sup>[22]</sup> By contrast, FT curves of 1T-MoS<sub>2</sub> exhibit a distinct decrease of the Mo–Mo bond length (short Mo–Mo bond) from 3.16 Å to 2.75 Å (Table 1), which corresponds to the characteristic bond length found in 1T phase MoS<sub>2</sub>.<sup>[24,25]</sup> Evidence for this feature can be also found by the larger Debye–Waller ( $\sigma^2$ ) factor of both Mo–S and Mo–Mo bonds in 1T phase compared to 2H-MoS<sub>2</sub> (see the Supporting Information, Table S1) although the normal Mo–Mo bond (3.16 Å) is still present in 1T.<sup>[24]</sup> Nevertheless, this shortened Mo–Mo bond disappeared after 24 h HER stability testing, which is consistent with the observations from XANES that 1T changes back to the 2H phase under these conditions. In the case of Am-MoS<sub>2</sub>, a similarly short Mo–S and Mo–Mo bond structure was found (Figure 2h, i). The similarities between the 1T and amorphous phases in XANES and EXAFS are also reflected in the Mo 3d core level and valence band photoemission spectra (Figure S3, Tables S2 and S3), shifting consistently to lower binding energies. Therefore, we may suggest that the short Mo–Mo bond

features observed in both 1T-MoS<sub>2</sub> and Am-MoS<sub>2</sub> play a key role in enhancing the HER activity of MoS<sub>2</sub> catalysts. Distinct from the 1T phase, the short Mo–Mo bond in Am-MoS<sub>2</sub> was retained after 24 h of HER stability testing. Considering the HER stability of Am-MoS<sub>2</sub>, we may conclude that the bond structure in Am-MoS<sub>2</sub> is intrinsic (viz. not caused by Li intercalation), resulting in a higher stability during 24 h HER stability testing.

Several structural models for amorphous MoS<sub>2</sub> or MoS<sub>3</sub> have been proposed in previous reports by for example, Hibble et al.<sup>[17b]</sup> and Weber et al.<sup>[11]</sup> However, based on our experimental observations, we cannot conclusively assign a structure to Am-MoS<sub>2</sub>. Nonetheless, the disorder in amorphous MoS<sub>2</sub> reported in this work is consistent with earlier reports.<sup>[17a,d]</sup> It is worth noting that even though the HER activity of 1T-MoS<sub>2</sub> decreases gradually (Figure 1d), the corresponding overpotential is still much lower than that of 2H-MoS<sub>2</sub>, which we have recently attributed to the presence of remaining Li adsorbed on the 1T-MoS<sub>2</sub> even after loss of intercalated Li.<sup>[18c]</sup> Inductively

**Table 1.** Summary of the ex situ grazing incidence Mo K-edge EXAFS spectroscopic features obtained for MoS<sub>2</sub> films under grazing incidence reflecting information about the top ≈ 3 nm of the material.<sup>[a]</sup>

Sample	Shell	Fresh		Spent	
		CN	R [Å]	CN	R [Å]
2H-MoS <sub>2</sub>	Mo–S	4.25	2.402	4.80	2.405
	Mo–Mo	2.26	3.155	2.98	3.158
1T-MoS <sub>2</sub>	Mo–S	3.06	2.419	5.86	2.365
	Mo–S (short)	1.78	2.019	–	–
	Mo–Mo	1.70	3.148	2.26	3.145
	Mo–Mo (short)	0.96	2.748	–	–
Am-MoS <sub>2</sub>	Mo–S	5.29	2.430	3.50	2.368
	Mo–S (short)	0.60	1.767	0.56	1.802
	Mo–Mo (short)	1.08	2.778	1.57	2.824

[a] Detailed fitting parameters can be found in Table S1.

coupled plasma optical emission spectroscopy (ICP-OES) analysis of MoS<sub>2</sub> films after stability tests confirms the presence of adsorbed Li on 1T-MoS<sub>2</sub> (Table S4), and the adsorption of Li on MoS<sub>2</sub> was observed to promote the activity of MoS<sub>2</sub>-catalyzed hydrogen evolution reaction in our recent work.<sup>[18c]</sup>

To follow the structural evolution of the different MoS<sub>2</sub> catalysts under HER conditions, an operando electrochemical cell (Figure S5) was developed and applied for X-ray absorption spectroscopy experiments. The operando EXAFS spectra of different MoS<sub>2</sub> polymorphs in dry state and at set potentials of +0.3 V and –0.3 V versus RHE in 0.1 M H<sub>2</sub>SO<sub>4</sub> are shown in Figure 3. Table 2 summarizes the EXAFS fitting results. It can be seen that, despite a small reduction in CN for the Mo–Mo shell, the Mo–Mo and Mo–S bond distances as well as the Mo–S CN remained the same within the accuracy range, pointing at the overall structural stability of 2H-MoS<sub>2</sub> under HER conditions. For both 1T and Am-MoS<sub>2</sub>, a shortened Mo–S bond could be identified as well. In contrast to the disappearance of short Mo–S and Mo–Mo bonds after the 24 h stability test (Figure 2), the operando EXAFS data of 1T-MoS<sub>2</sub> confirms the

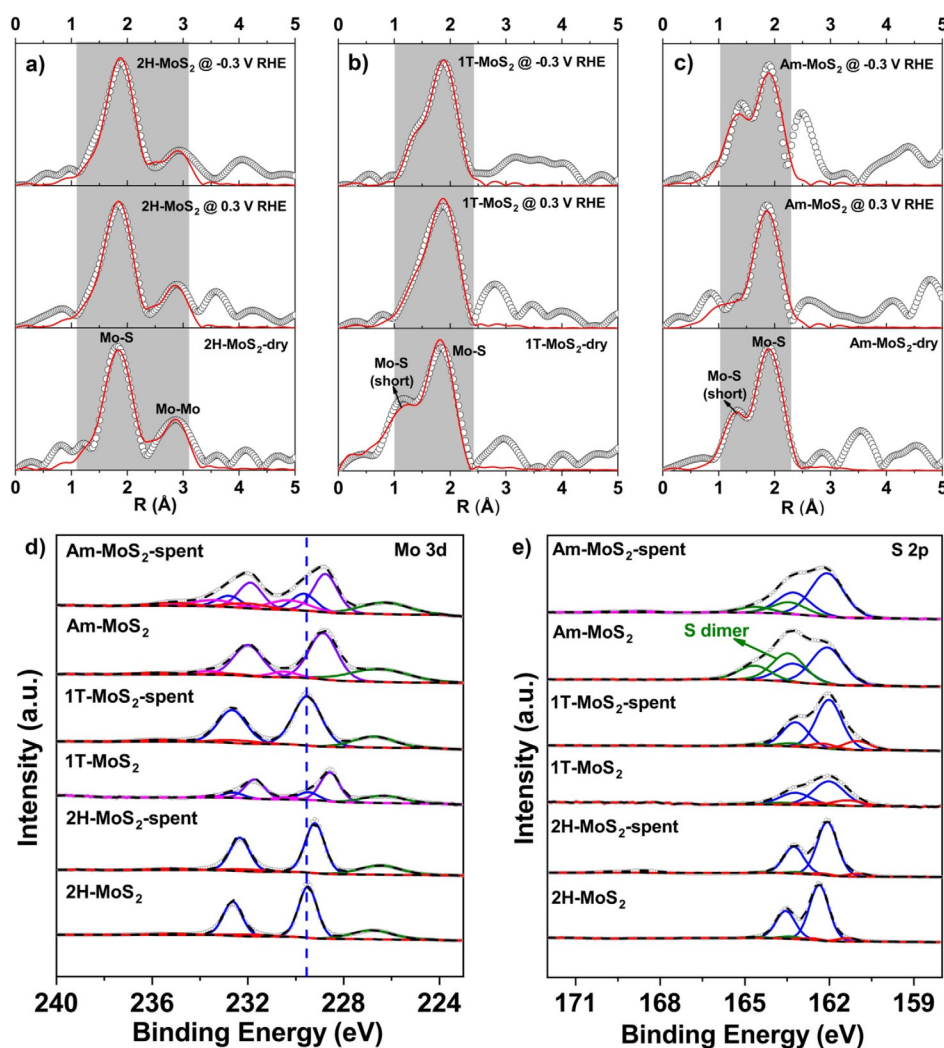


**Figure 3.** a–c) Mo K-edge Fourier transform EXAFS ( $k^2$ -weighted) of 2H- (a), 1T- (b), and Am- (c) MoS<sub>2</sub> under operando electrochemical conditions. Gray region represents R-range for fitting. d, e) X-ray photoemission spectra of Mo 3d (d) and S 2p (e) before and after (spent) operando XAS measurements.

**Table 2.** Summary of ex-situ grazing incidence Mo K-edge EXAFS spectroscopic features obtained for MoS<sub>2</sub> films under operando HER conditions.<sup>[a]</sup>

Sample	Shell	Dry		+ 0.3 V		− 0.3 V	
		CN	R [Å]	CN	R [Å]	CN	R [Å]
2H-MoS <sub>2</sub>	Mo–S	4.28	2.385	4.33	2.391	4.71	2.403
	Mo–Mo	3.06	3.154	2.70	3.142	2.11	3.165
1T-MoS <sub>2</sub>	Mo–S	6.66	2.354	5.82	2.416	3.78	2.406
	Mo–S (short)	5.90	2.004	0.96	1.835	0.34	1.827
Am-MoS <sub>2</sub>	Mo–S	4.60	2.443	3.04	2.401	2.30	2.407
	Mo–S (short)	0.36	1.775	0.38	1.644	0.58	1.795

[a] Detailed fitting parameters can be found in Table S5, S6, and S7.

retention of short Mo–S bonds under various potentials. On the one hand, the operando XAS was not carried out at grazing incidence angle and therefore reflects mostly bulk film information. On the other hand, the operando XAS measurements were performed at −0.3 V vs. RHE with a current density of only −200 μA cm<sup>−2</sup> (Figure S6), while the 24 hours stability tests were performed at −3 mA cm<sup>−2</sup>.

The surface electronic structures of 2H, 1T, and amorphous MoS<sub>2</sub> films were probed by XPS before and after operando XAS measurements (Figure 3 d, e). The Mo3d core level component describing the Mo–S bond for pristine 1T and Am-MoS<sub>2</sub> was shifted negatively by around 0.9 eV from that of the 2H phase, which is a characteristic feature for both 1T and amorphous phase MoS<sub>2</sub>.<sup>[18,26]</sup> However, the core level of Mo<sup>IV</sup>–S (Mo 3d<sub>5/2</sub> 228.6 eV) for 1T-MoS<sub>2</sub> shifted back to 229.5 eV after operando XAS tests, suggesting a transformation from 1T to 2H-MoS<sub>2</sub> at the surface. By contrast, the shift in Mo3d core level spectra for Am-MoS<sub>2</sub> (ca. 0.7 eV) remained unchanged after electrochemical tests (Figure 3 d). Raman spectroscopy was then used to further support the presence of different MoS<sub>2</sub> phases (Figure S18).<sup>[16]</sup> There is a redshift of E<sub>2g</sub><sup>1</sup> and A<sub>1g</sub> peaks for 1T-MoS<sub>2</sub> compared to those of 2H-MoS<sub>2</sub>, which stays constant before and after operando XAS measurements. The phase stability of the bulk 1T-MoS<sub>2</sub> film under mild reaction conditions is consistent with the EXAFS fitting results (Table 2). Even though sulfur dimers of Am-MoS<sub>2</sub> have been reported to be involved in proton reduction,<sup>[19c]</sup> the decreased intensity of sulfur dimers (Figure 3 e) here apparently did not influence the HER activity (Figure S6).

We utilized grazing incidence X-ray diffraction (GIXRD) to inspect the materials before and after operando XAS measurements. In the diffraction patterns of MoS<sub>2</sub> films (Figure S15), the diffraction peaks at 2θ = 14.2° (002) and 33.3° (101) indicative of 2H-MoS<sub>2</sub> are absent in the pristine 1T phase MoS<sub>2</sub> sample. However, the re-appearance of (002) and (101) reflections for the spent 1T-MoS<sub>2</sub> sample suggests that the material gradually changes back to 2H-MoS<sub>2</sub>. In addition, scanning electron microscopy (SEM) images (Figure S16) reveal obvious morphology changes for the 1T phase after HER tests. By contrast, neither Raman spectroscopy (Figure S18) nor GIXRD show any

peaks before and after HER testing for Am-MoS<sub>2</sub>. So far, we may conclude that even under mild HER conditions, the surface bond structure for the 1T phase would disappear and change back into the 2H phase, whereas amorphous MoS<sub>2</sub> retains its intrinsic short Mo–Mo bond feature and with that its high HER activity.

By using density functional theory (DFT), we compared the (electronic) structures of Mo<sub>3</sub>S<sub>9</sub> and Mo<sub>6</sub>S<sub>17</sub> clusters as a motif for Am-MoS<sub>2</sub> with those of 2H-MoS<sub>2</sub> and 1T-MoS<sub>2</sub> in order to understand differences in the Gibbs free energy of hydrogen adsorption (ΔG<sub>H\*</sub>), which is considered as a relevant descriptor for HER activity.<sup>[13b,27]</sup> The Mo–Mo and Mo–S bond distances found for the two small clusters correspond to those observed in 1T-MoS<sub>2</sub> and are shorter than those in 2H-MoS<sub>2</sub> (Figure 4 and Figures S21 and S22). Together with the structural data derived from EXAFS for our samples, this provides good grounds to hypothesize that Am-MoS<sub>2</sub> consists of small MoS<sub>x</sub> clusters with an increased S/Mo ratio and shortened Mo–Mo and Mo–S bonds, similar to what is known for crystalline 1T-MoS<sub>2</sub>. We then explored how these structures affect the HER performance for which we computed the Gibbs free energies of hydrogen adsorption (ΔG<sub>H\*</sub>, structures see Figures S23–S27).

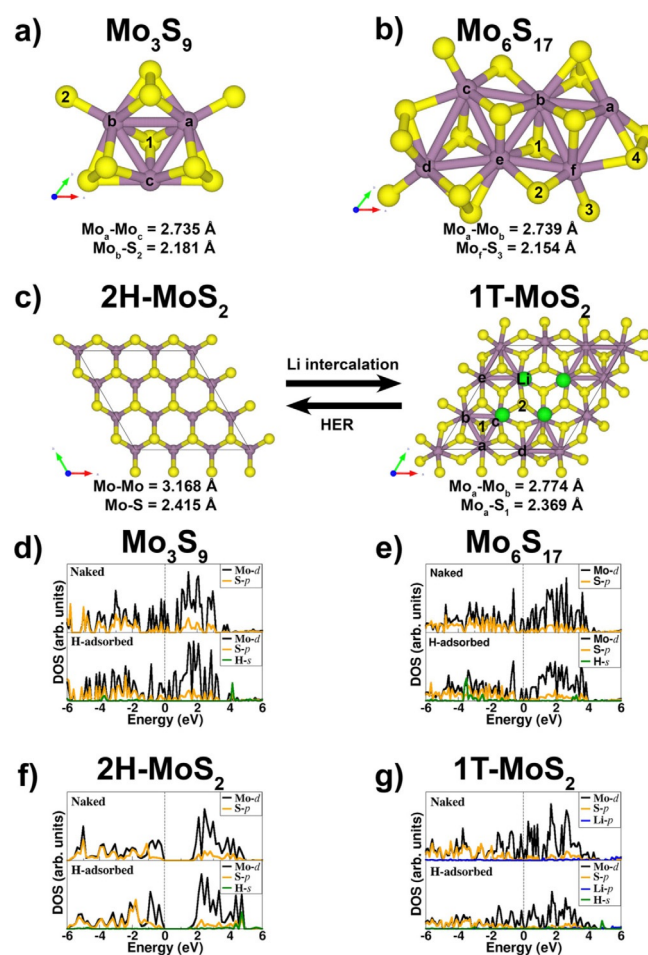


**Figure 4.** a, b) Optimized Mo<sub>3</sub>S<sub>9</sub> (a) and Mo<sub>6</sub>S<sub>17</sub> clusters serving as models for Am-MoS<sub>2</sub>; c) Schematic illustration of the structural evolution between crystalline 2H and 1T MoS<sub>2</sub> phases; normalized partial density of states (PDOS) of (d) Mo<sub>3</sub>S<sub>9</sub>, (e) Mo<sub>6</sub>S<sub>17</sub> clusters, (f) 2H-MoS<sub>2</sub>, and (g) 1T-MoS<sub>2</sub>.

For optimum HER activity, the value of  $\Delta G_{H^+}$  should be close to zero.<sup>[28]</sup> For  $\text{Mo}_3\text{S}_9$ , a  $\Delta G_{H^+}$  value of  $-0.06$  eV was computed, which is much more favorable than values of  $+2.13$  eV and  $+0.78$  eV for the basal planes of 2H- $\text{MoS}_2$  and Li-stabilized 1T- $\text{MoS}_2$ , respectively. As the hydrogen activation and formation on  $\text{MoS}_2$  is known to occur at the edge terminations,<sup>[9a,29]</sup> we also computed  $\Delta G_{H^+}$  for hydrogen adsorption on the Mo-edges of 2H- $\text{MoS}_2$  ( $-0.23$  eV) and 1T- $\text{MoS}_2$  ( $-0.10$  eV). These data confirm that the edges of the distorted 1T- $\text{MoS}_2$  phase are the preferred sites for HER in comparison to the edges of 2H- $\text{MoS}_2$  and further suggest that small clusters also have a favorable  $\Delta G_{H^+}$ . Figure 4 also gives the partial density of states (PDOS; Figure 4d–g) of the two investigated clusters, 1T- $\text{MoS}_2$  and 2H- $\text{MoS}_2$ . It can be immediately seen that, similar to 1T- $\text{MoS}_2$ , the  $\text{Mo}_3\text{S}_9$  and  $\text{Mo}_6\text{S}_{17}$  cluster models exhibit metallic character with their Fermi level crossing the Mo 3d orbitals. In contrast, 2H- $\text{MoS}_2$  is a semiconductor with a band gap of 1.59 eV, which is consistent with valence band spectroscopy (Figures S12 and S13) and earlier theoretical predictions.<sup>[30,31]</sup> The adsorption of hydrogen does not induce significant changes to the electronic structures, although coupling is observed between Hs orbital and Mo d and S p orbitals, consistent with weak bonding and high HER activity. The metallic nature of the  $\text{Mo}_3\text{S}_9$  and  $\text{Mo}_6\text{S}_{17}$  clusters and 1T- $\text{MoS}_2$  results in a higher intrinsic electronic conductivity for these materials than for the semiconducting 2H- $\text{MoS}_2$ . Therefore, in addition to a more optimum free energy for hydrogen adsorption, the enhanced HER activity of 1T- $\text{MoS}_2$  and Am- $\text{MoS}_2$  can be further rationalized by a higher intrinsic electronic conductivity.

In summary, we have provided both experimental and theoretical evidence for the importance of the short Mo–Mo bond structures of 1T and amorphous  $\text{MoS}_2$  in comparison to crystalline 2H- $\text{MoS}_2$  for explaining the higher HER performance. Whereas crystalline 1T- $\text{MoS}_2$  stabilized by intercalated  $\text{Li}^+$  also displays high performance, Li ions were found to dissolve in the electrolyte during electrochemical testing, resulting in a slow transformation back to the 2H- $\text{MoS}_2$  phase and a concomitant decrease in HER activity. In contrast, amorphous  $\text{MoS}_2$  retains much of its high HER activity during prolonged operation.

## Acknowledgements

This work is part of the program “CO<sub>2</sub>-neutral fuels” (project 13-CO26) of the Foundation for Fundamental Research on Matter (FOM), which was financially supported by the Netherlands Organization for Scientific Research (NWO). This research program was co-financed by Shell Global Solutions International B.V. A.S. and A.A.B. acknowledge financial support from the European Research Council (Grant Agreement No.648787-ALDof2DTMDs). Dr. Lu Gao and Jan Wiesfeld from Eindhoven University of Technology are thanked for their help in SEM measurements and 1T- $\text{MoS}_2$  preparation. Chunguang Chen and Prof. Dr. Peter H. L. Notten from Forschungszentrum Jülich, Germany are acknowledged for fruitful discussions.

## Conflict of interest

The authors declare no conflict of interest.

**Keywords:** bond structure · electrocatalysis · molybdenum · operando spectroscopy · polymorphism

- [1] a) D. Kong, J. J. Cha, H. Wang, H. R. Lee, Y. Cui, *Energy Environ. Sci.* **2013**, *6*, 3553–3558; b) J. Xie, J. Zhang, S. Li, F. Grote, X. Zhang, H. Zhang, R. Wang, Y. Lei, B. Pan, Y. Xie, *J. Am. Chem. Soc.* **2013**, *135*, 17881–17888; J. Xie, H. Zhang, S. Li, R. Wang, X. Sun, M. Zhou, J. Zhou, X. W. D. Lou, Y. Xie, *Adv. Mater.* **2013**, *25*, 5807–5813.
- [2] Y. Gong, Z. Liu, A. R. Lupini, G. Shi, J. Lin, S. Najmaei, Z. Lin, A. L. Elias, A. Berkdemir, G. You, H. Terrones, M. Terrones, R. Vajtai, S. T. Pantelides, S. J. Pennycook, J. Lou, W. Zhou, P. M. Ajayan, *Nano Lett.* **2014**, *14*, 442–449.
- [3] Y. Yu, G. H. Nam, Q. He, X. J. Wu, K. Zhang, Z. Yang, J. Chen, Q. Ma, M. Zhao, Z. Liu, F. R. Ran, X. Wang, H. Li, X. Huang, B. Li, Q. Xiong, Q. Zhang, L. Gu, Y. Du, W. Huang, H. Zhang, *Nat. Chem.* **2018**, *10*, 638–643.
- [4] K. K. Liu, W. Zhang, Y. H. Lee, Y. C. Lin, M. T. Chang, C. Y. Su, C. S. Chang, H. Li, Y. Shi, H. Zhang, C. S. Lai, L. J. Li, *Nano Lett.* **2012**, *12*, 1538–1544.
- [5] X. Wang, H. Feng, Y. Wu, L. Jiao, *J. Am. Chem. Soc.* **2013**, *135*, 5304–5307.
- [6] Y. Li, A. Yamaguchi, M. Yamamoto, K. Takai, R. Nakamura, *J. Phys. Chem. C* **2017**, *121*, 2154–2164.
- [7] a) L. van Haandel, E. J. M. Hensen, T. Weber, *Catal. Today* **2017**, *292*, 67–73; b) L.-A. S. Carlos, G. Morales-Guio, X. Hu, *Chem. Soc. Rev.* **2014**, *43*, 6555–6569.
- [8] a) J. D. Benck, T. R. Hellstern, J. Kibsgaard, P. Chakhranont, T. F. Jaramillo, *ACS Catal.* **2014**, *4*, 3957–3971; b) M. L. Tang, D. C. Grauer, B. Lassalle-Kaiser, V. K. Yachandra, L. Amirav, J. R. Long, J. Yano, A. P. Alivisatos, *Angew. Chem. Int. Ed.* **2011**, *50*, 10203–10207; *Angew. Chem.* **2011**, *123*, 10385–10389; c) Q. Ding, B. Song, P. Xu, S. Jin, *Chem* **2016**, *1*, 699–726.
- [9] a) T. F. Jaramillo, K. P. Jørgensen, J. Bonde, J. H. Nielsen, S. Hørch, I. Chorkendorff, *Science* **2007**, *317*, 100–102; b) J. C. B. H. Tributsch, *J. Electroanal. Chem.* **1977**, *81*, 97–111.
- [10] a) J. Kibsgaard, Z. Chen, B. N. Reinecke, T. F. Jaramillo, *Nat. Mater.* **2012**, *11*, 963–969; b) D. Kong, H. Wang, J. J. Cha, M. Pasta, K. J. Koski, J. Yao, Y. Cui, *Nano Lett.* **2013**, *13*, 1341–1347; c) C. Tsai, H. Li, S. Park, J. Park, H. S. Han, J. K. Nørskov, X. Zheng, F. Abild-Pedersen, *Nat. Commun.* **2017**, *8*, 15113.
- [11] T. Weber, J. C. Muijsers, J. W. Niemantsverdriet, *J. Phys. Chem.* **1995**, *99*, 9194–9200.
- [12] C. Backes, N. C. Berner, X. Chen, P. Lafargue, P. LaPlace, M. Freeley, G. S. Duesberg, J. N. Coleman, A. R. McDonald, *Angew. Chem. Int. Ed.* **2015**, *54*, 2638–2642; *Angew. Chem.* **2015**, *127*, 2676–2680.
- [13] a) D. Voiry, A. Goswami, R. Kappera, C. D. C. E. Silva, D. Kaplan, T. Fujita, M. Chen, T. Asefa, M. Chhowalla, *Nat. Chem.* **2015**, *7*, 45–49; b) X. Geng, W. Sun, W. Wu, B. Chen, A. Al-Hilo, M. Benamara, H. Zhu, F. Watanabe, J. Cui, T. P. Chen, *Nat. Commun.* **2016**, *7*, 10672.
- [14] a) Q. Tang, D.-e. Jiang, *ACS Catal.* **2016**, *6*, 4953–4961; b) Y. Yin, J. Han, Y. Zhang, X. Zhang, P. Xu, Q. Yuan, L. Samad, X. Wang, Y. Wang, Z. Zhang, P. Zhang, X. Cao, B. Song, S. Jin, *J. Am. Chem. Soc.* **2016**, *138*, 7965–7972.
- [15] a) W. Chen, J. Gu, Q. Liu, R. Luo, L. Yao, B. Sun, W. Zhang, H. Su, B. Chen, P. Liu, D. Zhang, *ACS Nano* **2018**, *12*, 308–316; b) M. Acerce, D. Voiry, M. Chhowalla, *Nat. Nanotechnol.* **2015**, *10*, 313–318.
- [16] S. J. R. Tan, S. Sarkar, X. Zhao, X. Luo, Y. Z. Luo, S. M. Poh, I. Abdelwahab, W. Zhou, T. Venkatesan, W. Chen, S. Y. Quek, K. P. Loh, *ACS Nano* **2018**, *12*, 5051–5058.
- [17] a) S. P. Cramer, K. S. Liang, A. J. Jacobson, C. H. Chang, R. R. Chianelli, *Inorg. Chem.* **1984**, *23*, 1215–1221; b) S. J. Hibble, D. A. Rice, D. M. Pickup, M. P. Beer, *Inorg. Chem.* **1995**, *34*, 5109–5113; c) M. de Boer, A. J. van Dillen, D. C. Koningsberger, J. W. Geus, *J. Phys. Chem.* **1994**, *98*, 7862–7870; d) J. Xie, Y. Xie, *ChemCatChem* **2015**, *7*, 2568–2580.
- [18] a) D. Merki, S. Fierro, H. Vrubel, X. Hu, *Chem. Sci.* **2011**, *2*, 1262–1267; b) C. G. Morales-Guio, X. Hu, *Acc. Chem. Res.* **2014**, *47*, 2671–2681; c) L.

- Wu, N. Y. Dzade, M. Yu, B. Mezari, A. J. F. van Hoof, H. Friedrich, N. H. de Leeuw, E. J. M. Hensen, J. P. Hofmann, *ACS Energy Lett.* **2019**, *4*, 1733–1740.
- [19] a) S. J. Hibble, G. B. Wood, *J. Am. Chem. Soc.* **2004**, *126*, 959–965; b) R. I. Walton, A. J. Dent, S. J. Hibble, *Chem. Mater.* **1998**, *10*, 3737–3745; c) B. Lassalle-Kaiser, D. Merki, H. Vrubel, S. Gul, V. K. Yachandra, X. Hu, J. Yano, *J. Am. Chem. Soc.* **2015**, *137*, 314–321; d) A. Sharma, M. A. Verheijen, L. Wu, S. Karwal, V. Vandalon, H. C. M. Knoop, R. S. Sundaram, J. P. Hofmann, W. M. M. Kessels, A. A. Bol, *Nanoscale* **2018**, *10*, 8615–8627.
- [20] a) X. Li, H.-Y. Wang, H. Yang, W. Cai, S. Liu, B. Liu, *Small Methods* **2018**, *2*, 1700395; b) N. Kornienko, J. Resasco, N. Becknell, C. M. Jiang, Y. S. Liu, K. Nie, X. Sun, J. Guo, S. R. Leone, P. Yang, *J. Am. Chem. Soc.* **2015**, *137*, 7448–7455.
- [21] J. W. Liwen, F. Wan, B. R. Perdue, T. T. Fister, S. Kim, C. A. Appleby, D. Prendergasta, *Phys. Chem. Chem. Phys.* **2016**, *18*, 17326–17329.
- [22] F. A. Lima, R. Bjornsson, T. Weyhermuller, P. Chandrasekaran, P. Glatzel, F. Neese, S. DeBeer, *Phys. Chem. Chem. Phys.* **2013**, *15*, 20911–20920.
- [23] J. Liu, R. E. Saw, Y. H. Kiang, *J. Pharm. Sci.* **2010**, *99*, 3807–3814.
- [24] Q. Liu, Q. Fang, W. Chu, Y. Wan, X. Li, W. Xu, M. Habib, S. Tao, Y. Zhou, D. Liu, T. Xiang, A. Khalil, X. Wu, M. Chhowalla, P. M. Ajayan, L. Song, *Chem. Mater.* **2017**, *29*, 4738–4744.
- [25] K. E. Dungey, M. D. Curtis, J. E. Penner-Hahn, *Chem. Mater.* **1998**, *10*, 2152–2161.
- [26] P. Afanasiev, H. Jovic, C. Lorentz, P. Leverd, N. Mastubayashi, L. Piccolo, M. Vrinat, *J. Phys. Chem. C* **2009**, *113*, 4139–4146.
- [27] Z. Zeng, Z. Yin, X. Huang, H. Li, Q. He, G. Lu, F. Boey, H. Zhang, *Angew. Chem. Int. Ed.* **2011**, *50*, 11093–11097; *Angew. Chem.* **2011**, *123*, 11289–11293.
- [28] P. D. Tran, T. V. Tran, M. Orio, S. Torelli, Q. D. Truong, K. Nayuki, Y. Sasaki, S. Y. Chiam, R. Yi, I. Honma, J. Barber, V. Artero, *Nat. Mater.* **2016**, *15*, 640–646.
- [29] a) J. K. Nørskov, T. Bligaard, A. Logadottir, J. R. Kitchin, J. G. Chen, S. Pandelov, U. Stimming, *J. Electrochem. Soc.* **2005**, *152*, J23–J26; b) J. Greeley, T. F. Jaramillo, J. Bonde, I. B. Chorkendorff, J. K. Nørskov, *Nat. Mater.* **2006**, *5*, 909–913.
- [30] a) M. R. Gao, M. K. Chan, Y. Sun, *Nat. Commun.* **2015**, *6*, 7493; b) X. Zhao, D. Fu, Z. Ding, Y. Y. Zhang, D. Wan, S. J. R. Tan, Z. Chen, K. Leng, J. Dan, W. Fu, D. Geng, P. Song, Y. Du, T. Venkatesan, S. T. Pantelides, S. J. Pennycook, W. Zhou, K. P. Loh, *Nano Lett.* **2018**, *18*, 482–490.
- [31] a) Q. Tang, D.-E. Jiang, *Chem. Mater.* **2015**, *27*, 3743–3748; b) X. Guo, G. Yang, J. Zhang, X. Xu, *ALP Adv.* **2015**, *5*, 097174; c) F. Xi, P. Bogdanoff, K. Harbauer, P. Plate, C. Höhn, J. Rappich, B. Wang, X. Han, R. van de Krol, S. Fiechter, *ACS Catal.* **2019**, *9*, 2368–2380.

---

 Manuscript received: July 3, 2019

Accepted manuscript online: July 18, 2019

Version of record online: August 8, 2019